JPP JOURNAL OF Pharmacy and Pharmacology
ROYAL PHARMACEUTICAL SOCIETY
JPP Journal of Pharmacy And Pharmacology
Research Paper

Investigation of process temperature and screw speed on properties of a pharmaceutical solid dispersion using corotating and counter-rotating twin-screw extruders

Justin M. Keen[a,b], Charlie Martin[c], Augie Machado[c], Harpreet Sandhu[d], James W. McGinity[a], James C. DiNunzio[d]

[a]College of Pharmacy, The University of Texas at Austin, Austin, [b]DisperSol Technologies, Georgetown, TX, [c]American Leistritz Extruder Corporation, Somerville, and [d]Pharmaceutical & Analytical R&D Department, Hoffmann-La Roche, Inc., Nutley, NJ, USA

Keywords
amorphous; dissolution; solid dispersion; thermal processing; twin-screw melt extrusion

Correspondence
Justin M. Keen, The University of Texas at Austin, 1 University Station, Mail Code A1902, Austin, TX 78712, USA.
E-mail: jmkeen@utexas.edu

Received February 14, 2013
Accepted June 15, 2013

doi: 10.1111/jphp.12106

Abstract

Objective The use of corotating twin screw hot-melt extruders to prepare amorphous drug/polymer systems has become commonplace. As small molecule drug candidates exiting discovery pipelines trend towards higher MW and become more structurally complicated, the acceptable operating space shifts below the drug melting point. The objective of this research is to investigate the extrusion process space, which should be selected to ensure that the drug is solubilized in the polymer with minimal thermal exposure, is critical in ensuring the performance, stability and purity of the solid dispersion.

Methods The properties of a model solid dispersion were investigated using both corotating and counter-rotating hot-melt twin-screw extruders operated at various temperatures and screw speeds. The solid state and dissolution performance of the resulting solid dispersions was investigated and evaluated in context of thermodynamic predictions from Flory–Huggins Theory. In addition, the residence time distributions were measured using a tracer, modelled and characterized.

Key findings The amorphous content in the resulting solid dispersions was dependent on the combination of screw speed, temperature and operating mode.

Conclusions The counter-rotating extruder was observed to form amorphous solid dispersions at a slightly lower temperature and with a narrower residence time distribution, which also exhibited a more desirable shape.

Introduction

Hot-melt extrusion (HME) has emerged as a robust processing technology in the pharmaceutical industry where it is used to produce a variety of dosage forms including granules, pellets, tablets, transdermal laminates, implants, and process intermediates for controlled release and solubility enhancement of therapeutics.[1–4] Twin-screw extruders are routinely employed due to their ability to form intimate mixtures of drugs and polymers. Corotating and counter-rotating twin-screw extruders are both used to melt, shear and pump polymeric materials. However, their differing geometries change the relative amounts of positive displacement and shear. In terms of plastics processing and broadly speaking, corotating extruders are widely employed to mix plastic formulations for subsequent use in injection molding or subsequent extrusion processes. Counter-rotating extruders are often, but not exclusively, employed for processes requiring stable or high-pressure output, such as forming continuous profiles or sheets. The counter-rotating extruder provides a greater degree of positive displacement and extensional shear occurs along the entire length of the screw, even in the conveying sections.[5] On the other hand, corotating extruders are perceived to offer a wider range of mixing capabilities.[6] However, there is a great deal of overlap in the processing capabilities of the two extrusion modes as screw designs can be designed for either mode to accomplish a wide range of pressure and shear profiles.

Corotating twin-screw extruders are routinely employed for solubility enhancement of Biopharmaceutics Classification System class II and IV drugs. The properties of small molecule drugs emerging from development pipelines during the last decade indicate a trend towards higher MW, increasing lipophilicity and lower solubility.[7] With this trend in drug molecule properties, the configuration of the

extruder and its operating conditions becomes more critical in ensuring that these drugs are solubilized in the polymer during the residence time in the extruder. In particular, as higher MWs correspond to higher melting points, melting the drug during the process may become prohibited by the operating range of the polymer. Keserü and Makara[7] also observed that drug candidates are becoming more complex, having increased numbers of heavy atoms, rotors, and rings. Undoubtedly, these attributes lead to increased sensitivity to degradation in the amorphous state or upon melting further pressuring the process to operate at lower temperatures.

For thermally sensitive high MW drugs, the balance between mixing efficiency and thermal exposure must be evaluated and controlled to ensure safety and efficacy of the final product. In theory, counter-rotating extruders may offer an advantage for this application, for two reasons: (1) counter-rotating extruders impart extensional flow along the entire length of the screw because of the diverging geometry at the intermesh, and (2) counter-rotating extruders can be designed to provide a greater degree of positive displacement.

The flow profiles in twin-screw extruders are complex, yet there are a few key distinctions. Maximum velocity occurs at the intermeshing region of a counter-rotating extruder and at the tips of the screws in the corotating extruder.[8] In the counter-rotating extruder, material is stretched and elongated at the interface as the surfaces of the screws diverge. The resulting extensional flow increases the interfacial area exponentially with time, while in a simple shear field, interfacial area grows linearly with time.[9,10] From the perspective of a drug particle dissolving in a polymer melt, this flow profile may prove important in reducing the boundary layer thickness and increasing the dissolution rate of the drug. The dissolution process of crystalline drugs in polymer melts has been demonstrated as a critical aspect of producing amorphous solid dispersions below the melting point of the drug.[11,12]

Another important consequence of the screw geometries of counter-rotating versus corotating twin-screw extruders is that the counter-rotation configuration, depending on screw design, provides positive displacement instead of semidrag flow that is indicative of corotating extruders.[13] In practical terms, counter-rotation designs can be configured more like a pump and can have a narrower residence time distribution (RTD). During solid dispersion development as with all pharmaceutical products, low-level impurities from thermal degradation must be monitored to ensure safety and efficacy of the final dosage form.[14] Impurity formation during thermal processing is a known function of residence time.[15]

The objective of this study was to investigate the properties of a model solid dispersion system of griseofulvin (GRIS) and copovidone (Kollidon® VA 64) in a Leistritz 27 mm twin-screw extruder operated in the corotating and counter-rotating mode. GRIS was selected due to its poor solubility, MW of 353 Da and a melting point >200 °C; properties that are in-line with pipeline molecules that require solubility enhancement. Relative to HME, these properties indicate that the drug will require solubilization in the polymer and will not be melted during extrusion. This initial investigation focuses on the extrusion mode and parameters required to dissolve crystalline GRIS into the solid dispersion and to quantify the RTD of the two geometries. The temperature, screw speed and concentration of GRIS in the solid dispersion were varied for each extrusion mode to compare and contrast the factors leading to an amorphous solid dispersion. These factors were considered in parallel to the thermodynamic predictions of Flory–Huggins Theory for this system. The *in vitro* performance of the amorphous solid dispersions and the solid state were investigated. Finally, the RTDs for each extruder configuration were determined, modelled and characterized.

Materials and Methods

Materials

Copovidone, Kollidon VA 64, was kindly donated by BASF Corporation (Florham Park, NJ, USA). Micronized GRIS was purchased from Letco Medical (Decatur, AL, USA). Indigo carmine was obtained from Acros Organics (Geel, Belgum). HPLC grade acetronitrile and tetrahydrafuran were purchased from Fisher Scientific (Pittsburg, PA, USA). All materials were used as supplied.

Hot-melt extrusion

GRIS and copovidone were simultaneously fed at a combined feed rate of 4 kg/h, from two separate gravimetric twin-screw feeders, (K-Tron, Pitman, NJ, USA) to a 27-mm twin-screw extruder, Leistritz Micro 27 (Leistritz, Somerville, NJ, USA). The composition of the feed was varied based on the test condition between 20% and 40% by weight GRIS. Experiments were conducted both with the gear box and screws configured for corotation (GL) and for counter-rotation (GG). The screw designs, both 40 : 1 length : diameter, are included in Figure 1 for reference. The barrel temperature, starting at the first mixing zone, was set at the test temperature. The extruder was equipped with a 5-mm diameter die that was maintained at 160 °C for all experiments. The screw rpm, along with the feed composition, and barrel temperature were varied to investigate the conditions that yielded amorphous extruded based on visual observation. The test conditions evaluated are listed in Table 1. The total feed rate for all tests was 4 kg/h, and the extrudate was air-cooled on

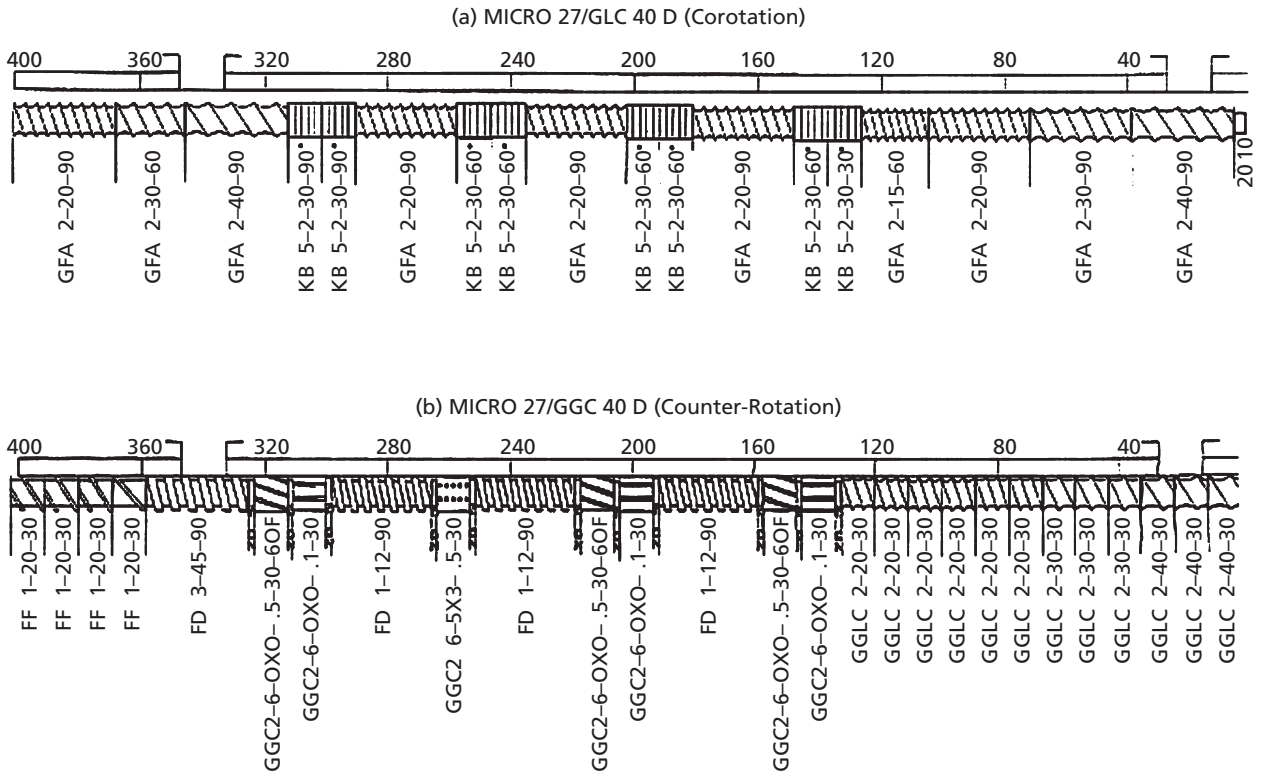

Figure 1 Twin-screw designs. Screw design employed in the Leistritz 27 mm twin screw extruder for (a) corotating configuration and the (b) counter-rotating configuration.

Table 1 Extrusion test conditions

Test No.	Extruder configuration	Drug load (%)	Temperature (°C)	Screw speed (rpm)	Visual assessment of extrudate
1	Corotating	20	160	150	Crystalline
2	Corotating	20	180	150	Amorphous
3	Corotating	30	170	300	Crystalline
4	Corotating	30	170	450	Crystalline
5	Corotating	30	180	150	Crystalline
6	Corotating	30	180	300	Crystalline
7	Corotating	30	180	450	Amorphous
8	Corotating	40	180	450	Crystalline
9	Counter-Rotating	20	160	150	—
10	Counter-Rotating	20	160	300	Amorphous
11	Counter-Rotating	30	160	300	Crystalline
12	Counter-Rotating	30	170	300	Crystalline
13	Counter-Rotating	30	170	450	Amorphous
14	Counter-Rotating	30	180	300	Crystalline
15	Counter-Rotating	30	180	450	Amorphous

Extrusion test conditions and results of the visual assessment.

a conveyor. Collected samples were ground using a coffee mill to transform to powder. The size fraction between 90 and 180 μm, which is a suitable particle size for the intended analytical evaluations and ease of handling, was collected for further analysis.

X-ray powder diffraction

An Equinox 100 standalone bench top X-ray diffractometer (INEL, Inc., Stratham, NH, USA) was used to analyse the milled extrudate samples for the presence of crystallinity.

Samples were placed in an aluminum crucible and loaded in a rotating sample holder. Samples were analysed for 300 s using a Cu K radiation source ($\lambda = 1.5418$ Å) operating at 42 kV and 0.81 mA.

Shear cell analysis

To evaluate the powder flow behaviour of the GRIS/copovidone system, 20% and 30% GRIS by weight were blended and analysed using a RST-XS Ring Shear Tester (Dietmar Schulze, Wolfenbüttel, Germany). The shear stress of both blends was evaluated under load ranging from 0.3 to 1.2 kPa. The flow-function coefficient (FFC) was determined using RSV 95 software (Dietmar Schulze).

Thermal analysis

Thermal analysis was performed using a model Q20 modulated differential scanning calorimeter (mDSC) (TA Instruments, New Castle, DE, USA) to determine the influence of copovidone on the onset melting temperature and the melting enthalpy of GRIS and investigate the glass transition temperature of test samples. Physical mixtures of 100%, 95%, 90%, 85% and 80% GRIS by volume were prepared, stored in a desiccator and tested in triplicate. The 6.0 ± 0.1 mg samples were analysed under a nitrogen atmosphere (50 ml/min). The samples were equilibrated at 35 °C for 5 min followed by a 1.00 °C/min ramp to 250 °C. The glass transition temperature of the test samples was determined on 6.0 ± 1 mg samples. The samples were equilibrated at 35 °C for 5 min followed by a 5 °C/min ramp to 250 °C modulating every 60 s at an amplitude of 1 °C. Glass transition temperatures were measured similarly for determining the concentration Tg profile with the exception that samples were pretreated by heating to 250 °C and quench-cooled to remove thermal history.

A Thermogravimetric Analyzer 7 (Perkin-Elmer, Norwalk, CT, USA) was used to investigate the thermal stability of GRIS. Sample pans were placed in the chamber and equilibrated at 50 °C under a constant flow of nitrogen (65 ml/min). Once equilibrated, the sample mass was monitored as the temperature was increased from 50 to 350 °C at a rate of 10 °C/min.

Rheology

The viscosity of copovidone as a function of indigo carmine concentration (0.00%, 0.25%, 0.50% and 1.00% w/w indigo carmine) was determined using an Advanced Rheometer 2000 (TA Instruments) equipped with a smooth parallel plate assembly. Samples were prepared by blending copovidone and indigo carmine, then extruding at 160 °C and 360 rpm using a HAAKE Minilab II Microcompounder (Thermo Electron Corporation, Newington, NH, USA). Ground samples were raised to 155 °C and incrementally squeezed to a gap clearance of 2000 µm in the rheometer. The system was equilibrated for 10 min before reducing the clearance to 1000 µm, followed by additional 10 min of equilibration. Testing was performed in Oscillatory Frequency Sweep mode with a frequency range of 0.1–100 Hz at a constant strain amplitude in the linear viscoelastic region. Samples attained steady-state to allow for the decay of transient phenomena before measurement. Data were transformed using the Cox Merz rule within the TA Advantage Software.

Dissolution

Nonsink dissolution analysis was performed using a VK 7010 dissolution testing apparatus (Varian, Inc., Palo Alto, CA, USA) configured according to USP XXXIX Method A (paddle method). Sieved extrudate was weighed to achieve 50 ± 1 mg GRIS and added to dissolution vessels containing 1000 ml 0.1 N HCl. The vessels were maintained at 37.0 ± 0.5 °C with paddles rotating at 50 rpm. Test samples were studied in triplicate, with 5-ml samples collected from the vessels at 5, 10, 15, 30, 45, 60, 90 and 120 min. Immediately following sampling, the samples were filtered through 0.2 µm, 17 mm, polyvinylidene difluoride syringe filters (Fisher Scientific, Pittsburgh, PA, USA) and diluted 1 : 1 with 50 : 50 acetonitrile : water and transferred to HPLC vials for analysis.

High-performance liquid chromatography

HPLC was used to analyse the potency of selected test samples as well as to quantitate the dissolution samples. A 717 autosampler (Waters Corporation, Milford, MA, USA) configured with a Luna 5 µm CN 100 Å, 150 × 4.6 mm column (Phenomenex, Torrance, CA, USA). The mobile phase was a mixture of acetonitrile : water : tetrahydrafuran 65 : 35 : 5 flowing at 1.00 ml/min. Potency samples were prepared to contain 0.1 mg/ml in acetonitrile:water 50 : 50. Potency and dissolution samples were injected at volume of 20 µl. A Waters 2996 photodiode array detector, extracting at 292 nm, was used to quantify the results. The retention time of GRIS was approximately 4 min. All analyses maintained linearity ($R^2 = 0.999$) in the range tested and a relative standard deviation of less than 2.0%. Empower Version 5.0 was utilized to process all chromatography data.

Flory–Huggins Theory

The phase diagram for the GRIS and copovidone system was generated using Flory–Huggins Theory, as described previously.[16–22] The Gibbs free energy of mixing function that results from application of the Flory–Huggins model is dependent on the volume fraction of the drug, ϕ, a constant

indicative of the relative size of the polymer in relation to the drug, m, and the interaction parameter, χ.

$$\frac{\Delta G_{mix}}{RT} = \phi \ln \phi + \frac{(1-\phi)}{m} \ln(1-\phi) + \phi(1-\phi)\chi \qquad (1)$$

DSC experiments to determine the melting enthalpy of the drug, ΔH, and either the melting temperature,[18,19] onset of melting[20] or ending of melting[21] have been applied by various authors to determine χ, which is a function of temperature.[23] For the GRIS/copovidone system, melting temperature was selected based on the reproducibility of this value in experimental trials. The equation to determine χ in the drugs melting range is:

$$\frac{1}{T_m} - \frac{1}{T_m^o} = \phi \ln \phi + \frac{(1-\phi)}{m} \ln(1-\phi) + \phi(1-\phi)\chi \qquad (2)$$

Where T_m^o is the melting point of GRIS and T_m is the melting point of GRIS in the presence of copovidone at each concentration studied. The constant, m, was determined from the MWs of GRIS and copovidone along with their density, ρ,

$$m = \frac{\frac{MW_{copovidone}}{\rho_{copovidone}}}{\frac{MW_{GRIS}}{\rho_{GRIS}}} \qquad (3)$$

The temperature dependency of χ can be extrapolated to room temperature with the application of solubility parameters.[20] Literature values for the Hoftyzer and Van Krevelen solubility parameters, δ, for GRIS, 29.54 $(J/cm^3)^{1/2}$,[24] and copovidone, 23.91 $(J/cm^3)^{1/2}$,[20] along with the molar volume per Flory–Huggins lattice site, υ, taken to be the molar volume of GRIS, 255.1 cm^3/mol,[22,25]

$$\chi = \frac{\nu(\delta_{GRIS} - \delta_{copovidone})^2}{RT} \qquad (4)$$

The results from Equations 2 and 4 were combined to determine the overall dependence of χ from 25 °C to the melting point for the drug.

$$\chi(T) = A + \frac{B}{T} \qquad (5)$$

It is notable that for this analysis χ is assumed to be only a function of temperature. Any dependency on composition is neglected; this assumption is in line with that made by previous authors.[18–21] With the solution to Equation 5, a Gibbs free energy diagram at selected temperatures can be produced.

Setting the second derivative of Equation 1 equal to 0 and determining ϕ as a function of χ allows for the determination of the boundary between unstable and metastable regions, the spinodal curve.

$$\frac{1}{\phi} + \frac{1}{m(1-\phi)} - 2\chi = 0 \qquad (6)$$

Furthermore, the boundary between the metastable and stable regions can be formed by constructing the common tangents between minima on the free energy diagram. This corresponds to points in which the chemical potentials of two phases are in equilibrium.

$$\left(\frac{\partial \frac{G}{RT}}{\partial \varnothing}\right)^{Phase\ 1} = \left(\frac{\partial \frac{G}{RT}}{\partial \varnothing}\right)^{Phase\ 2} \qquad (7)$$

and

$$\left(\frac{\partial \frac{G}{RT}}{\partial (1-\varnothing)}\right)^{Phase\ 1} = \left(\frac{\partial \frac{G}{RT}}{\partial (1-\varnothing)}\right)^{Phase\ 2} \qquad (8)$$

The binodal curve resulting from the solution to Equations 7 and 8, which is solved numerically, will intersect the spinodal curve at the critical point, the third derivative of Equation 1.

$$\frac{\partial^3 \frac{G}{RT}}{\partial \phi^3} = 0 \qquad (9)$$

However, it is notable that in the case of a small molecule drug and a high-MW polymer (large value of m), the free energy curves and spinodal curve are highly asymmetrical. Consequently, a real solution to Equations 7 and 8 may not exist. From a physical perspective, this situation arises when the metastable form separates into two phases in which one phase consists of pure drug. In this case, the binodal curve in the region of interest can be constructed from the single minimum observed on the free energy curves.

Residence time distribution

The RTD was determined for the corotating and counter-rotating extrusion configurations by charging 1 g of indigo carmine into the extruder feed hopper. The charge was selected based on the results of preliminary studies performed with copovidone on a 16-mm NANO 16 corotating twin-screw extruder (Leistritz). The time at which material was charged into the feed zone was denoted as $t = 0$ and a calibrated timer utilized to determine the time. The time at

which coloured extrudate emerged from the die was noted, and samples were subsequently collected every 15 s for 2 min after the initial colouring was visually observed. After that point, sampling frequency was reduced to 1-min intervals for a total of 10 min. Approximately 50 cm of extrudate was collected at each time point. Samples were evaluated in triplicate by dissolving 150 ± 50 mg of neat extrudate in 20 ml of acetonitrile : water 50 : 50 and quantified using a ultraviolet (UV) spectrometer (μQuant, BIO-TEK® Instruments, Inc., Winooski, VT, USA) at 610 nm. The UV response of indigo carmine in this analysis was linear over the concentration range studied ($R^2 > 0.9999$), and the limit of detection was 0.25 μg/ml.

The data were fit according to the Zusatz RTD function.[26,27]

$$E(t) = at^{-c-1}b^{c+1}e^{\left(b^c t^c - 1\right)\left(\frac{-c-1}{c}\right)} \tag{10}$$

Where *a*, *b* and *c* are fitted parameter for the system. Mu and Thompson[28] recently demonstrated the applicability of this approach to modelling complex screw geometry where mixing sections result in axial dispersion observed as tailing of the RTD. The RTD in this case was fitted assuming additive contributions from the conveying and mixing zones. Mathematically, the RTD equation is fitted by deconvoluting a modified form of Equation 10, which is modified to be a summation of each contributor, $n = 3$ was used for our analysis.

$$E(t) = \sum_i^n \left(at^{-c-1}b^{c+1}e^{\left(b^c t^c - 1\right)\left(\frac{-c-1}{c}\right)} \right)_i \tag{11}$$

The mean residence time is calculated from the first moment of the distribution,

$$t_{mean} = \int_0^\infty tE(t)dt \tag{12}$$

and the variance is calculated from the second moment.[29]

$$\sigma^2 = \int_0^\infty (t - t_{mean})^2 E(t)dt \tag{13}$$

The skewness[30] is calculated to describe the asymmetry of the RTD.

$$S = \sigma^{-3} \int_0^\infty (t - t_{mean})^3 E(t)dt \tag{14}$$

Results and Discussion

Thermal analysis and construction of the phase diagram

The GRIS melting point was observed to decrease with increasing concentration of copovidone (Figure 2). The Flory–Huggins interaction parameter, χ, was calculated by

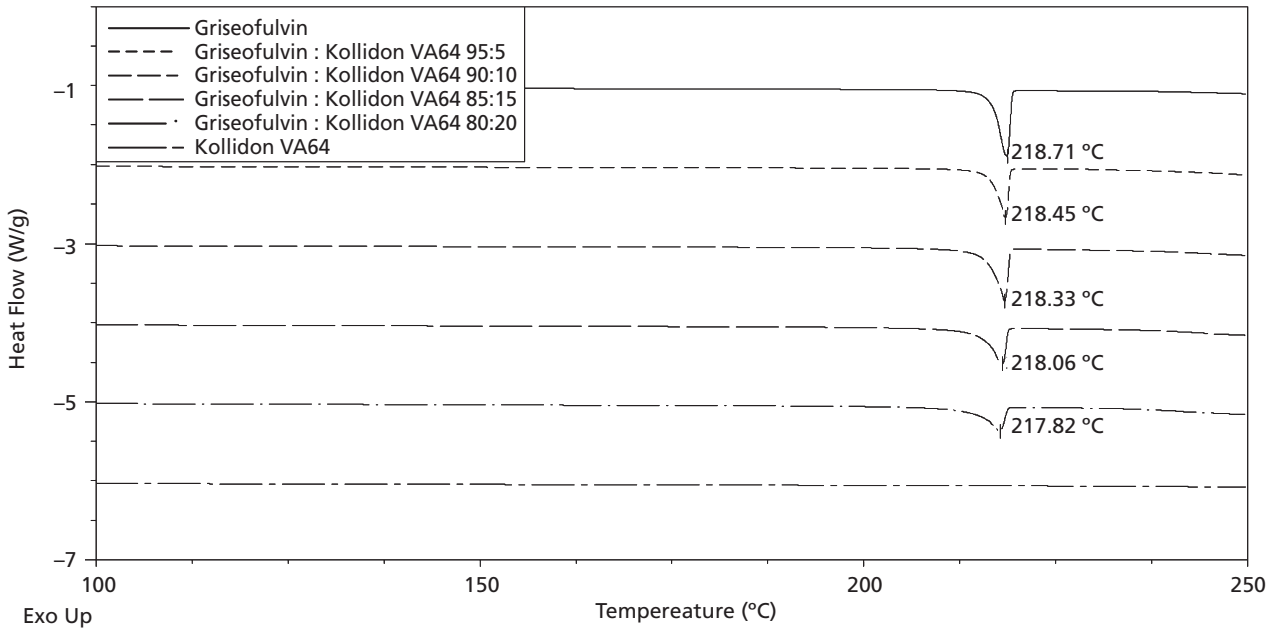

Figure 2 Melting point depression. Differential scanning calorimetry thermograms for physical mixtures of griseofulvin : copovidone over the range of 100 : 0 to 80 : 20 by volume demonstrating the melting point depression as observed scanning at 1 °C/min.

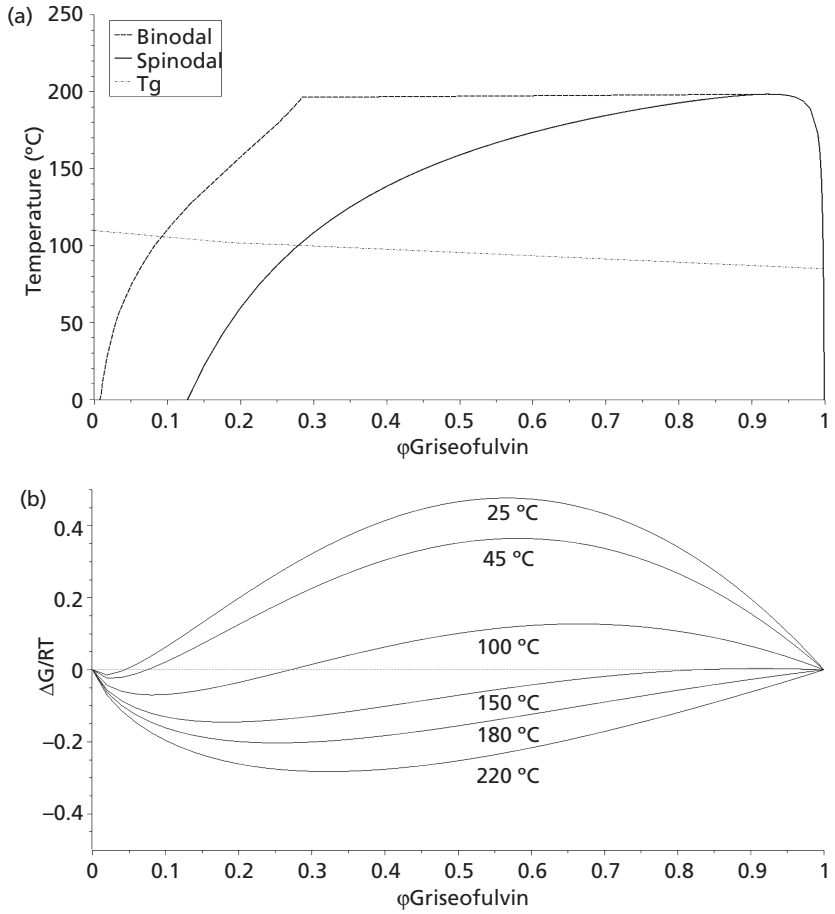

Figure 3 Free energy and phase diagrams. (a) Thermal phase diagram of the griseofulvin/copovidone representing the boundaries between thermodynamically unstable, metastable and stable regions as bounded by the spinodal and binodal curves along with the glass transition boundary. (b) Free energy diagram of the griseofulvin/copovidone system as determined using Flory–Huggins Theory.

melting point depression data at elevated temperature (Equation 2) and by solubility parameter estimation at 25 °C, resulting in values of 0.4 ± 0.08 and 3.6, respectively. The decrease of χ at elevated temperature indicated mixing of GRIS and copovidone becomes more favourable with increasing temperature. Examination of free energy diagrams presented in Figure 3a and generated by the solving the free energy relationship (Equation 1) at specific temperatures further highlight this behaviour, with thermodynamic favourability for systems greater than 60% v/v at 150 °C. Conversely, at low temperatures, only limited thermodynamic favourability is observed, with systems less than 5% v/v being favoured at room temperature.

The free energy diagram, presented in Figure 3b, was used to generate a phase diagram for the GRIS : copovidone system, illustrating the stable, metastable and unstable regions of the system as a function of temperature. In addition to the binodal and spinodal curves, the glass transition temperature curve serves as an indicator of a drastic change in viscosity,[31] where below this line reduced molecular motion of the system kinetically hinders mixing of thermodynamically favourable systems and demixing of thermodynamically unfavourable systems on experimentally relevant timescales.[32] As temperature increases, viscosity decreases, driving an increase of molecular motion within the system that reduces kinetic barriers in attaining thermodynamic equilibrium. While rates to achieve equilibrium can be reduced from months to minutes by increasing molecular mobility, when considering processes on extrusion-relevant timescales, kinetic factors cannot be neglected. For pharmaceutical applications, residence times generally range from 5 s to 10 min depending on extruder process design and operating conditions. To successfully develop amorphous dispersions by HME, it is necessary to identify drug loadings that do not lie in the unstable region at the target processing conditions. From the phase diagram, 20% and 30% w/w GRIS concentration are projected to be obtained at melt temperatures of 159 and 198 °C, respectively. Noting

that the melting point of the drug substance is 219 °C, the phase diagram estimates establish the lower bound for melt temperature that can achieve the target drug loading in the solubilization regime.

Thermal stability of a compound is also a critical property that can establish an upper bound to allowable melt temperature. During thermal analysis, GRIS was observed to be thermally stable in comparison with similar-size molecules we have encountered in development. GRIS degradation beyond 0.1% was observed at temperatures greater than 200 °C (data not presented), with an increasing rate of decomposition noted as temperature increased. Copovidone decomposition has also been reported at temperatures exceeding 230 °C.[33] Based on these results, all efforts should be made to minimize melt temperatures to less than 200 °C. As such, processing the previous data, the GRIS melting temperature is not possible, and the extrusion process must dissolve the drug in the polymer melt. In this case, the processing conditions and mixing modalities control dissolution of drug in the molten polymer.[11,12]

Effect of processing modes and processing conditions on griseofulvin/copovidone solid dispersions

Different processing modalities have been utilized in twin-screw extrusion, but the application of counter-rotating extruders for pharmaceutical systems remains limited. To make a direct assessment of the performance of corotating extruders and counter-rotating extruders in a head-to-head comparison, process geometries were developed in a similar fashion. Across the length of each screw, four major sections of dispersive and distributive elements were placed, having a total common length across both systems to reduce equipment setup bias during the comparative trials. To further assess the impact of process parameters on the performance of the system, systems containing 20% and 30% GRIS were extruded under the conditions shown in Table 1.

At-line visual observations were made about the appearance of the dispersions, noting the well-documented tendency of amorphous dispersions to form a clear glass during the extrusion process. For simple systems, an amorphous solid dispersion will have a transparent appearance, and significant levels of crystallinity impart an opaque appearance to the solid dispersion.[34] Using the corotating extruder, opaque, semicrystalline solid dispersions were produced at processing temperatures of 160 °C and 150 rpm. Under similar conditions with the counter-rotating extruder, it was not possible to achieve sufficient feed into the extruder, preventing a direct comparison between the systems for generating solid dispersions. However, comparison between feed intake behaviours can be made. For the counter-rotating mode, the screws rotate outward on top and inward at the bottom; this maximizes the free volume for intake.[35] The powder must flow down into the lower wedge formed by the screws and conveyed. In the corotating mode, powder is transferred from one screw towards the other where it is further conveyed. In this mode, the wedge area provides a twist-restraint, which reduces the tendency of rotation in the channel and increases particle conveyance in the axial direction. The difference of intake mechanism based on equipment geometry most likely contributed to the observed performance difference.

Micronized GRIS and copovidone used in these trials have specific attributes that can impact flow into the feed section of the extruder. The low particle size of the drug substance presents a problem for powder flow, providing a high specific surface area for interaction and low individual particle mass that reduce flowability into the open area of the screw flights for transport into the closed barrel. Copovidone also exhibits characteristics that can impact flow, particularly the moisture content of the material and tendency to form sticky gels in high-moisture environments. Characterization of flow properties was performed using shear cell analysis of the 20% and 30% by weight GRIS blends, although the materials were fed independently. FFC values of 8.04 and 6.37, respectively, were noted, which indicated moderate flow for a pharmaceutical system. Based on the trend of the FFC, increasing the GRIS concentration degrades the flowability of the formulation, indicating that the particle size may heavily influence the feed intake. Given the common properties of this system with many pharmaceutical systems, the poor intake performance on a counter-rotating extruder may occur with a range of pharmaceutical systems.

Increasing screw speed to 300 rpm enhanced the conveyance of the counter-rotating feed section to support a feed rate of 4 kg/h, indicating that greater screw speed could be used to compensate for lower conveying efficiency of the counter-rotating system. Furthermore, it was observed that a clear glass was formed, indicating amorphous extrudate at 160 °C. In comparison with the corotating extruder that required a process section temperature of 180 °C, an amorphous form was achieved at a process section temperature 20 °C lower with the counter-rotating unit. This suggested a potential benefit in solubilization of high melting point active pharmaceutical ingredients in the molten polymer, although the contribution of greater screw speed in the counter-rotating system to this performance is likely significant. Performance differences between the two systems were also investigated using a 30% GRIS formulation. A similar procedure of incremental temperature and screw speed increases were followed to identify the conditions under which an amorphous form was produced. For operating conditions at or below 170 °C process section temperature and 300 rpm, an opaque, semicrystalline extrudate was

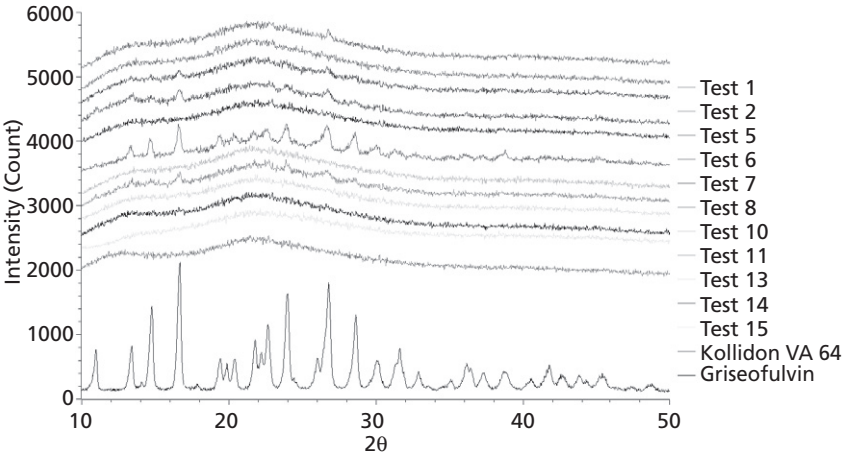

Figure 4 X-ray diffractograms. Powder X-ray diffractograms of griseofulvin, copovidone and selected test samples over the range of 10–50° 2θ.

observed. Further increasing the screw speed for both systems to 450 rpm allowed the counter-rotating system to achieve a transparent glass, while the corotating system remained opaque. For the corotating configuration, increasing process temperature to 180 °C was necessary to establish an amorphous form while maintaining a screw speed of 450 rpm. Interestingly, operation of the counter-rotating extruder at 180 °C and 450 rpm resulted in an amorphous system; however, by reducing the screw speed to 300 rpm, a semicrystalline system was observed. By lowering the speed, the energy imparted by the screws for dissolution was decreased. This suggested that mechanical energy input was the more dominant factor in solubilizing the high-melting-point compound in the molten polymer when compared with process section temperature. This result was not entirely unexpected, as it is well known in extrusion that mechanical energy contributes to the majority of heat energy produced in the system,[36] with the process section functioning as a sink to remove thermal energy. Furthermore, the mechanical energy input varies based on the aggressiveness of the screw elements selected and their distribution along the screw. It should also be noted that the dissolution process of drug in molten polymer is a kinetic phenomenon tied to the RTD of the process and the boundary layer thickness at the drug-polymer interface, which is a function of mixing and driving force for dissolution as determined by the equilibrium solubility of drug in polymer. Although not possible to identify the primary mechanism that limited dissolution at the lower screw speed, it is clear that screw speed had a more dominant influence on achieving complete melt solubilization than process section temperature.

Direct comparison of the corotating and counter-rotating extruders operated at 180 °C and 450 rpm produced dispersions with similar visual characteristics, yielding clear amorphous glasses. Pressure build-up and viscous dissipation have been reported to contribute to localized heating in the extruder. To better characterize local heating in these systems, the melt temperature was measured directly by placement of a thermocouple into the screw tip region near die outlet. The observed melt temperatures for the counter-rotating and corotating extruders were 196 ± 4 °C and 204 ± 4 °C, respectively. Comparing the process section temperature for the 20% drug loading formulation and melt temperatures measured for the 30% drug loading formulation to the phase diagram, Figure 3b, show that the compositions lie in close proximity to the binodal curve. This suggests that the maximum attainable drug loading of a high-melting-point compound in a specific system is given by the binodal boundary at the operating melt temperature.

Upon cooling, the solid dispersion transitions the metastable region and Tg boundary shown in the phase diagram, to where both 20% and 30% GRIS dispersions exist in the unstable region where the high viscosity of the polymer provides kinetic stabilization. The Tg boundary was generated from second run mDSC analysis of copovidone, GRIS and X-ray amorphous compositions of 20% and 30% w/w, the slope of the line indicates that the GRIS : copovidone system lacks significant specific interactions and exhibits volume additivity.[37] Over time, this system will eventually relax[32] and establish an equilibrium defined by the binodal curve, with a component of pure crystalline drug. To investigate the amorphous nature of the extrudates, powder X-ray diffraction analysis was performed on representative test samples shown in Figure 4. The results of the cooled extrudates corroborated the results observed from visually observing the melt with one exception. Test 14 was observed to have opaque character during extrusion trials, yet no peaks were observed by X-ray. The most likely explanation

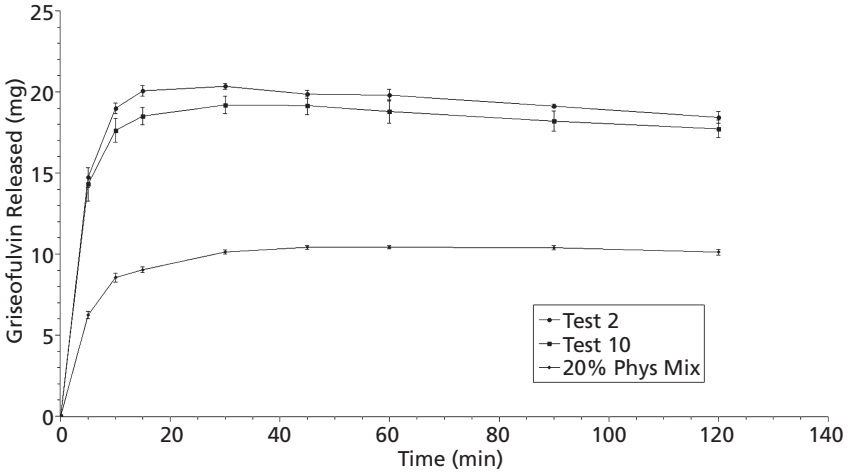

Figure 5 Nonsink dissolution of 20% griseofulvin solid dispersions. Nonsink dissolution of 20% by weight griseofulvin solid dispersions and a physical mixture of griseofulvin and copovidone. $n = 3$, 50 mg griseofulvin per vessel in 1000 ml of 0.1 N HCl at 37 °C and 50 rpm.

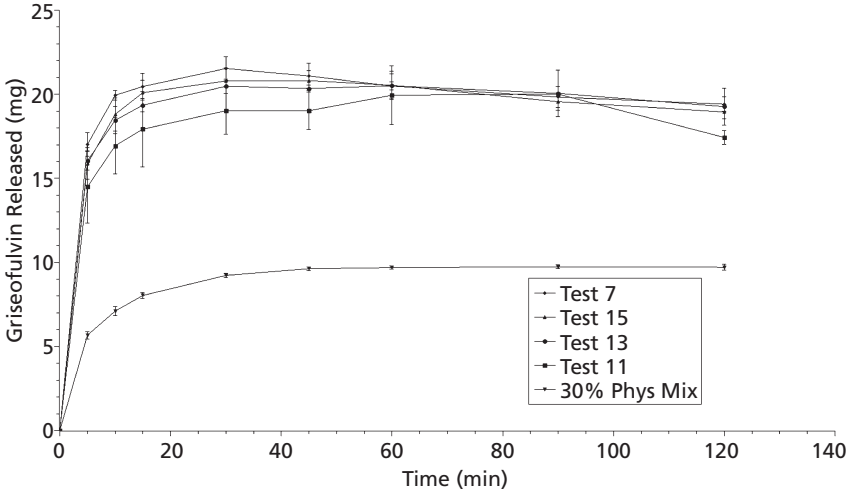

Figure 6 Nonsink dissolution of 30% griseofulvin solid dispersions. Nonsink dissolution of 20% by weight griseofulvin solid dispersions and a physical mixture of griseofulvin and copovidone. $n = 3$, 50 mg griseofulvin per vessel in 1000 ml of 0.1 N HCl at 37 °C and 50 rpm.

is that the amount of crystalline material was below the limit of detection, which was determined by serial dilution of physical mixtures of GRIS and copovidone to be < 1.25% w/w of crystalline material in the sample.

Nonsink dissolution was performed on the extrudates from selected tests to ascertain if the process geometry affected the drug release behaviour of the dispersions. In some cases, the supersaturating capability of solid dispersions *in vitro* is an indicator of *in vivo* exposure.[38] This type of testing can also be used as a quality metric to assess levels of residual crystallinity within formulations. The 20% by weight compositions, Figure 5, and the 30% by weight compositions, Figure 6, that were determined to be amorphous both visually and by X-ray were found to exhibit similar rates and extent of supersaturation. Properties of the dissolution curves are summarized in Table 2. Solution concentrations greater than twofold improvements over the physical mixtures were observed. In addition, a sample from test 11, which was observed to be crystalline by X-ray was investigated and included along with the X-ray amorphous compositions in Figure 6. The results indicate that the presence of crystalline GRIS slowed the rate of supersaturation, while the maximum level of supersaturation was similar to that of the amorphous compositions. Furthermore, the 90- and 120-min data points indicate that the crystalline GRIS induced a greater degree of precipitation. All samples tested for dissolution were also confirmed to have acceptable potency, similar purity to that of the standard, similar glass

Table 2 Dissolution attributes

Sample description	S_{max}	Initial dissolution $rate_{0–5\ min}$ (mg/min)	$AUDC_{0–120\ min}$ (mg min)
Test 2	1.95 ± 0.01	2.94 ± 0.12	2267 ± 31
Test 10	1.84 ± 0.05	2.86 ± 0.20	2154 ± 74
20% physical mixture	—	1.24 ± 0.09	1170 ± 38
Test 7	2.20 ± 0.07	3.40 ± 0.14	2375 ± 76
Test 11	2.05 ± 0.04	2.90 ± 0.42	2217 ± 137
Test 13	2.10 ± 0.04	3.20 ± 0.11	2329 ± 78
Test 15	2.13 ± 0.06	3.17 ± 0.18	2331 ± 78
30% physical mixture	—	1.13 ± 0.04	1083 ± 14

Maximum supersaturation relative to the physical mixture, dissolution rate at 5 min and area under the dissolution curve.

transition temperature and loss on drying values (data not shown).

Residence time distribution

Residence time of continuous operations are often characterized through the use of a tracer, which in the case of extrusion is a material added as a single bolus charge into the feed zone where the concentration of tracer in the extrudate is measured as a function of time on leaving the die. The tracer selected for the RTD tests, indigo carmine, has a large chromaphore, allowing detection by UV even at low solution concentration and at a wavelength that does not overlap with GRIS or copovidone. This enables charging the tracer at a low mass compared with the feed rate of the solid dispersion. Indigo carmine is a crystalline material, with a high melting point (>235 °C) that dissolves in the polymer at the extrusion temperatures employed, mimicking the behaviour of GRIS in the system. Furthermore, indigo carmine allows for visual observation of the RTD, which transitions from a dark indigo, to blue, to a light green hue as the concentration decreases, allowing accurate sample collection and determination of the minimum exit time. While these attributes of the tracer are ideal, there is still a possibility that a small molecule tracer could act as a plasticizer and alter the melt viscosity such that the normal flow profiles are disturbed. To rule this out, the rheology of copovidone in the presence of up to 1% indigo carmine was measured, Figure 7. Based on these results, indigo carmine is not a plasticizer for copovidone and is acceptable for the intended purpose.

According to Poulesquen and Vergnes,[29] the RTD of an extrusion system can be summarized by three attributes, the minimum exit time, the mean residence time and the variance of the distribution. However, in the case of thermally sensitive materials, it may also be important to look at the third moment of distribution for the purpose of characterizing the skewness, which is often characterized for plug flow reactors[30] and in this case provides a value to describe the asymmetry of the RTD. The primary parameters affecting the mean residence time are the feed rate, screw design and the internal free volume of the extruder. For a given extruder volume and feed rate, the skewness gives an indication to the propensity for tailing, which should be minimized to reduce drug exposure to high temperatures to a minimum.

Test conditions 7 and 15, representing the 30% w/w GRIS solid dispersions produced at 180 °C and 450 rpm for the corotating and counter-rotating configurations, respectively, were selected for the RTD trials. The results are plotted in Figure 8 along with the nonlinear least squares fit to Equation 11. The results for the moments for the distribution and other key statistics are summarized in Table 3. Based on these results, the RTD of the solid dispersion for both configurations exhibited similar minimum exit times, within 5 s of each other. The mean residence time, variance and asymmetry were all reduced for the counter-rotation configuration when compared with the corotating configuration. The counter-rotating extruder also provided shorter t_{90} and t_{99} values, which denote the time that 90% and 99% of the charge has passed through the extruder. Together, these values represent a potential benefit for using a counter-rotating extruder when working with heat-sensitive or high-melting-point compounds. The narrower distribution presented by the counter-rotating platform allows for more uniform processing of material. For high-melting-point compounds where the drug must be solubilized in the molten polymer, this helps to ensure that dissolution is achieved with minimal excess energy input. Similarly, for high-melting-point compounds where decomposition occurs as a function of time and temperature, the narrow distribution and more uniform time exposures seen in the counter-rotating system should minimize impurity formation. This suggests a potential underutilized benefit of counter-rotating extruders for the production of solid dispersions.

Conclusion

In this investigation, a counter-rotating and corotating twin-screw extrusion comparison was performed with a focus on the impact of the critical attributes of the solid dispersion. Both configurations produced visually and X-ray amorphous solid dispersions of up to 30% GRIS in copovidone having similar supersaturating capability. However, under the parameters of this study, the counter-rotating configuration produced the solid dispersion at a reduced temperature and with a RTD that minimized the mean

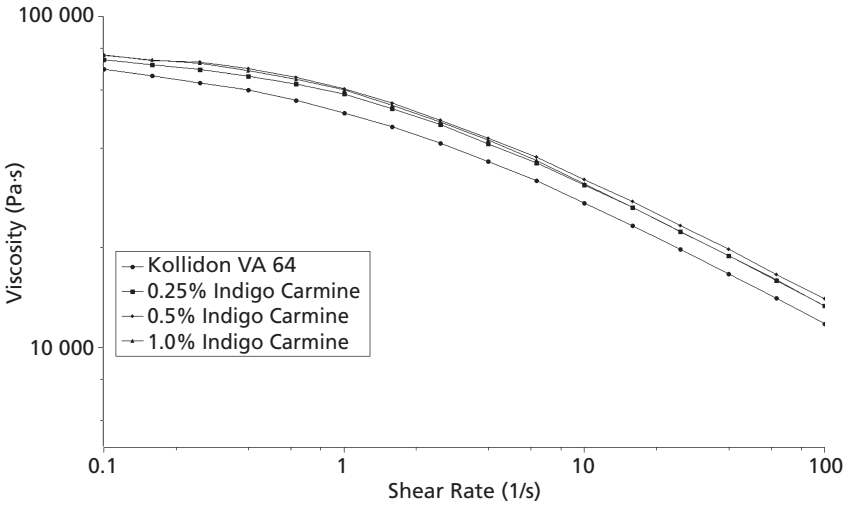

Figure 7 Viscosity of copovidone with tracer. Viscosity of copovidone as measured at 155 °C in the presence of the tracer, indigo carmine, used in the residence time distribution study.

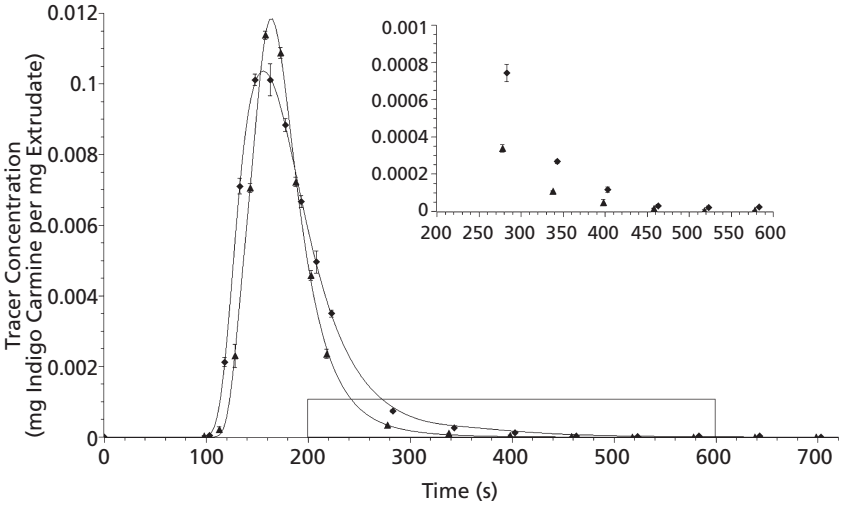

Figure 8 Residence time distributions. Residence time distribution of 30% griseofulvin solid dispersion at 4 kg/h, 450 rpm, 180 °C for (◆) corotating and (▲) counter-rotating configurations in a Leistritz 27 mm extruder, boxed area shown in inset.

residence time, variance and skewness when compared with the corotating configuration. Using these attributes of counter-rotating extruders, it may be possible to address challenging poorly soluble drug candidates where uniformity or minimization of thermal exposure are critical to the processing strategy.

Table 3 Residence time distribution attibutes

RTD attribute	Corotation	Counter-rotation
Minimum exit time	103 s	98 s
Mean residence time	189 s	178 s
Variance	3473 s^2	1265 s^2
Skewness	2.40	2.14
T90	252 s	219 s
T99	417 s	300 s

Moments of the residence time distributions for the corotating and counter-rotating 27-mm twin-screw extrusion trials as measured at 180 °C and 450 rpm following a 1 g indigo carmine tracer charged to a 30% w/w griseofulvin in copovidone extrusion process operating at 4 kg/h.

Declarations

Conflict of interest

The Authors declare that they have no conflicts of interest to disclose.

Acknowledgements

The authors would like to thank Hoffmann-La Roche, Inc. for their financial support for the project, BASF for donation of copovidone, Connor J. Foley for his assistance with dissolution analysis, and American Leistritz Extruder Corporation for providing the equipment and facilities for the RTD studies.

References

1. Repka MA *et al*. Pharmaceutical applications of hot-melt extrusion: part II. *Drug Dev Ind Pharm* 2007; 10: 1043–1057.
2. Terife G *et al*. Hot melt mixing and foaming of soluplus® and indomethacin. *Polym Eng Sci* 2012; 8: 1629–1639.
3. Dierickx L *et al*. Co-extrusion as manufacturing technique for fixed-dose combination mini-matrices. *Eur J Pharm Biopharm* 2012; 3: 683–689.
4. Feng J *et al*. Evaluation of polymer carriers with regard to the bioavailability enhancement of bifendate solid dispersions prepared by hot-melt extrusion. *Drug Dev Ind Pharm* 2012; 6: 735–743.
5. Tadmor Z, Gogos CG. *Principles of Polymer Processing*. Hoboken: Wiley-Interscience, 2006.
6. Crowley MM *et al*. Pharmaceutical applications of hot-melt extrusion: part I. *Drug Dev Ind Pharm* 2007; 9: 909–926.
7. Keserü GM, Makara GM. The influence of lead discovery strategies on the properties of drug candidates. *Nat Rev Drug Discov* 2009; 3: 203–212.
8. Shah A, Gupta M. Comparison of the flow in co-rotating and counter-rotating twin-screw extruders. *ANTEC, Conference Proceedings*. 2004: 443–447.
9. Tucker IIIC. Mixing of miscible liquids. In: Manas-Zloczower I, ed. *Mixing and Compounding of Polymers*. Munich: Hanser Publications, 2009: 5–38.
10. Manas-Zloczower I. Continuous process visualization: visual observation, on-line monitoring, model-fluid extrusion and simulation. In: Manas-Zloczower I, ed. *Mixing and Compounding of Polymers*. Munich: Hanser Publications, 2009: 473–572.
11. Liu H *et al*. Effects of extrusion process parameters on the dissolution behavior of indomethacin in Eudragit® E PO solid dispersions. *Int J Pharm* 2010; 1-2: 161–169.
12. Hughey JR *et al*. Thermal processing of a poorly water-soluble drug substance exhibiting a high melting point: the utility of KinetiSol® dispersing. *Int J Pharm* 2011; 1–2: 222–230.
13. Martin C. *Counter-Rotating Twin-Screw Extruders. SPE Plastics Technician's Toolbox – Extrusion, Drawer 4: Single & Twin-Screw Extruders, Section: Twin Screw Extruders*. Denton, TX: RonJon Publishing, 2004: 101–106.
14. Guidance for industry: Q3A impurities in new drug substances. *Revision 2*. Center for Drug Evaluation and Research (CDER), 2008.
15. DiNunzio JC *et al*. Fusion production of solid dispersions containing a heat-sensitive active ingredient by hot melt extrusion and Kinetisol® dispersing. *Eur J Pharm Biopharm* 2010; 2: 340–351.
16. Flory PJ. Thermodynamics of high polymer solutions. *J Chem Phys* 1942; 10: 51–61.
17. Huggins ML. Thermodynamics properties of solutions of long-chain compounds. *Ann N Y Acad Sci* 1942; 1: 1–32.
18. Marsac P *et al*. Estimation of drug–polymer miscibility and solubility in amorphous solid dispersions using experimentally determined interaction parameters. *Pharm Res* 2009; 1: 139–151.
19. Lin D, Huang Y. A thermal analysis method to predict the complete phase diagram of drug-polymer solid dispersions. *Int J Pharm* 2010; 1-2: 109–115.
20. Zhao Y *et al*. Prediction of the thermal phase diagram of amorphous solid dispersions by Flory–Huggins theory. *J Pharm Sci* 2011; 8: 3196–3207.
21. Tian Y *et al*. Construction of drug–polymer thermodynamic phase diagrams using Flory–Huggins interaction theory: identifying the relevance of temperature and drug weight fraction to phase separation within solid dispersions. *Mol Pharm* 2012; 1: 236–248.
22. Bellantone RA *et al*. A method to predict the equilibrium solubility of drugs in solid polymers near room temperature using thermal analysis. *J Pharm Sci* 2012; 12: 4549–4558.
23. Marsac P *et al*. Theoretical and practical approaches for prediction of drug–polymer miscibility and solubility. *Pharm Res* 2006; 10: 2417–2426.
24. Nair R *et al*. Influence of various drugs on the glass transition temperature of poly(vinylpyrrolidone): a thermodynamic and spectroscopic investigation. *Int J Pharm* 2001; 1–2: 83–96.
25. Al-Obaidi H *et al*. Characterization and stability of ternary solid dispersions with PVP and PHPMA. *Int J Pharm* 2011; 1–2: 20–27.
26. Poulesquen A *et al*. A study of residence time distribution in co-rotating twin-screw extruders. Part II: experimental validation. *Polym Eng Sci* 2003; 12: 1849–1862.
27. Zhang X-M *et al*. Local residence time, residence revolution, and residence volume distributions in twin-screw extruders. *Polym Eng Sci* 2008; 1: 19–28.
28. Mu B, Thompson MR. Examining the mechanics of granulation with a hot melt binder in a twin-screw extruder. *Chem Eng Sci* 2012; 0: 46–56.
29. Poulesquen A, Vergnes B. A study of residence time distribution in co-rotating twin-screw extruders. Part I: theoretical modeling. *Polym Eng Sci* 2003; 12: 1841–1848.
30. Minnich CB *et al*. Bridging the gap: a nested-pipe reactor for slow reactions in continuous flow chemical synthesis. *Chem Eng J* 2011; 2: 759–764.

31. Craig DQM *et al*. The relevance of the amorphous state to pharmaceutical dosage forms: glassy drugs and freeze dried systems. *Int J Pharm* 1999; 2: 179–207.
32. Hancock BC *et al*. Molecular mobility of amorphous pharmaceutical solids below their glass transition temperatures. *Pharm Res* 1995; 6: 799–806.
33. Kolter K *et al*. *Hot-Melt Extrusion with BASF Pharma Polymers: Extrusion Compendium*. Ludwigshafen, Germany: BASF, 2010.
34. Forster A *et al*. Characterization of glass solutions of poorly water-soluble drugs produced by melt extrusion with hydrophilic amorphous polymers. *J Pharm Pharmacol* 2001; 3: 303–315.
35. Eise K *et al*. An analysis of twin-screw extruder mechanisms. *Adv Polym Tech* 1981; 2: 18–39.
36. Breitenbach J. Melt extrusion: from process to drug delivery technology. *Eur J Pharm Biopharm* 2002; 2: 107–117.
37. Hancock BC, Zografi G. The relationship between the glass transition temperature and the water content of amorphous pharmaceutical solids. *Pharm Res* 1994; 4: 471–477.
38. Newman A *et al*. Assessing the performance of amorphous solid dispersions. *J Pharm Sci* 2012; 4: 1355–1377.